Role of the nucleotidyl cyclase helical domain in catalytically active dimer formation

Irene Vercellino[a], Lenka Rezabkova[a], Vincent Olieric[b], Yevhen Polyhach[c], Tobias Weinert[a], Richard A. Kammerer[a], Gunnar Jeschke[c], and Volodymyr M. Korkhov[a,d,1]

[a]Laboratory of Biomolecular Research, Division of Biology and Chemistry, Paul Scherrer Institute, 5232 Villigen, Switzerland; [b]Macromolecular Crystallography Group, Paul Scherrer Institute, 5232 Villigen, Switzerland; [c]Laboratory of Physical Chemistry, Swiss Federal Institute of Technology in Zurich (ETH Zurich), 8093 Zurich, Switzerland; and [d]Institute of Biochemistry, ETH Zurich, 8093 Zurich, Switzerland

Edited by Gregory A. Petsko, Weill Cornell Medical College, New York, NY, and approved October 10, 2017 (received for review July 17, 2017)

Nucleotidyl cyclases, including membrane-integral and soluble adenylyl and guanylyl cyclases, are central components in a wide range of signaling pathways. These proteins are architecturally diverse, yet many of them share a conserved feature, a helical region that precedes the catalytic cyclase domain. The role of this region in cyclase dimerization has been a subject of debate. Although mutations within this region in various cyclases have been linked to genetic diseases, the molecular details of their effects on the enzymes remain unknown. Here, we report an X-ray structure of the cytosolic portion of the membrane-integral adenylyl cyclase Cya from *Mycobacterium intracellulare* in a nucleotide-bound state. The helical domains of each Cya monomer form a tight hairpin, bringing the two catalytic domains into an active dimerized state. Mutations in the helical domain of Cya mimic the disease-related mutations in human proteins, recapitulating the profiles of the corresponding mutated enzymes, adenylyl cyclase-5 and retinal guanylyl cyclase-1. Our experiments with full-length Cya and its cytosolic domain link the mutations to protein stability, and the ability to induce an active dimeric conformation of the catalytic domains. Sequence conservation indicates that this domain is an integral part of cyclase machinery across protein families and species. Our study provides evidence for a role of the helical domain in establishing a catalytically competent dimeric cyclase conformation. Our results also suggest that the disease-associated mutations in the corresponding regions of human nucleotidyl cyclases disrupt the normal helical domain structure.

adenylyl cyclase | helical domain | dimerization | Cya | X-ray structure

The nucleotidyl cyclases convert nucleoside triphosphates (ATP or GTP) into cyclic nucleotides (cAMP or cGMP), the ubiquitous second messenger molecules involved in a broad range of signaling pathways (1). All mammalian adenylyl cyclases (ACs) and guanylyl cyclases (GCs) utilize the type III cyclase domain fold in various architectures. Catalytic domain dimerization is a prerequisite of the cyclase function: Substrate and allosteric binding sites are located at the cyclase domain dimer interface (2, 3). The nine membrane AC types in mammals (AC1–9) are polytopic membrane proteins with 12 transmembrane (TM) domains that are regulated by heterotrimeric G proteins (4). The TM domains 1–6 and 7–12 are followed by short helical domains and catalytic domains; although the structures of the catalytic domains bound to G protein α subunit have been solved (5), the role of the adjacent domains in the membrane ACs remains unclear. The only soluble AC in mammals, AC10 (or sAC), is a G protein-insensitive enzyme regulated by carbonate and involved in a multitude of physiological processes (6). Two short helical motifs precede each of the catalytic domains in AC10 polypeptide (6). Mammalian membrane receptor GCs contain an N-terminal receptor ectodomain, followed by a single transmembrane helix, a kinase-like domain, and a cyclase domain (7). A helical domain is located between the kinase-like domain and the cyclase domain within the polypeptide of a receptor GC, and appears to be involved in dimerization of the catalytic domain and in GC activation (8). Soluble GC is a receptor for nitric oxide (NO) and a key protein in NO-signaling pathways (9). This protein is a heterodimer composed of two subunits, each containing a heme-nitric oxide/oxygen (H-NOX) domain, a Per-Arnt-Sim (PAS) domain, an extended helical domain, and a cyclase domain (10, 11). Thus, in the repertoire of enzymes generating cyclic nucleotides, the helical domain and the catalytic domain are the unifying components, yet the focus of the majority of structural studies to date has been primarily on the catalytic domains. The structure and functional significance of the helical domain has until now remained largely unexplored.

Disruption of cAMP or cGMP production underlies a number of genetic diseases. For example, multiple mutations have been found in adenylyl and guanylyl cyclases (AC5 and retGC1, respectively) that are associated with movement disorders, such as familial diskynesia with facial myokymia (FDFM) (12, 13), cone-rod dystrophy (CORD6) (14), autosomal dominant progressive cone degeneration (15), and Leber congenital amaurosis (LCA-1) (16). The known disease-linked mutations in retGC1 are spread throughout the whole sequence of the protein and span all of its domains (14–17). Fewer mutations have been identified in the soluble regions of AC5, such as R418W or A726T (12, 18). Importantly, the helical domains of both enzymes contain the "hotspots" for disease-relevant mutations (such as the residues R418 in AC5 and R838 in retGC1). The occurrence of pathological amino

Significance

Adenylyl and guanylyl cyclases are at the core of cellular signaling. Although the molecular mechanisms of the reactions catalyzed by these enzymes are well established, their structures and biophysical properties remain only partially characterized. Here, we report the structure of the cytosolic domain of a mycobacterial adenylyl cyclase Cya, an evolutionary ancestor of mammalian membrane adenylyl cyclases. The structure reveals the helical domain, a highly conserved structural element that links the catalytic and transmembrane portions of Cya. We show how helical domains bring together the catalytic domains to form functionally active dimers. Our data suggest that the disease-linked mutations in human nucleotidyl cyclases may disrupt the correct assembly of the helical domain, preventing the formation of an active dimeric enzyme.

Author contributions: I.V. and V.M.K. designed research; I.V., L.R., V.O., Y.P., and V.M.K. performed research; I.V., L.R., V.O., Y.P., T.W., R.A.K., G.J., and V.M.K. analyzed data; and I.V., Y.P., G.J., and V.M.K. wrote the paper.

The authors declare no conflict of interest.

This article is a PNAS Direct Submission.

Data deposition: The atomic coordinates and structure factors have been deposited in the Protein Data Bank, www.wwpdb.org (PDB ID codes 5O5K and 5O5L).

[1]To whom correspondence should be addressed. Email: volodymyr.korkhov@psi.ch.

This article contains supporting information online at www.pnas.org/lookup/suppl/doi:10.1073/pnas.1712621114/-/DCSupplemental.

acid substitutions in this short amino acid sequence upstream of catalytic domains of ACs and GCs suggests that the helical domain is critically important for function of nucleotidyl cyclases in general. The consequences of the disease-linked mutations on the organism level have been described, but the mechanisms underlying these effects are unclear.

Structural information pertaining to membrane-integral ACs has until now been largely limited to the structures of catalytic domains of mammalian AC in a complex with G protein αs subunit (5, 19, 20). These structures provided great insights into the molecular mechanism of cAMP production and its regulation by the G protein α subunit, small molecules, and ions. In addition, structures of monomeric catalytic domain of trypanosoma membrane ACs (21) and of dimeric catalytic core of a *Pseudomonas aeruginosa* CyaB (22) have been reported. However, the role of the adjacent domains in assembly of a functional AC has until now remained unclear: Neither the TM domains, nor the juxtamembrane soluble regions of the membrane ACs, have been functionally and structurally characterized.

Mycobacterial Cya occupies a special niche within the superfamily of nucleotidyl cyclases. The Cya homolog from *M. tuberculosis*, Rv1625c, has been proposed to be a distant evolutionary ancestor to mammalian membrane-integral ACs based on architectural similarity between these proteins (23). Cya homologs are composed of a 6-TM helical bundle, followed by a helical domain and a type III catalytic domain (23, 24). Dimerization is thought to bring the two halves of the enzyme together, reconstituting a mammalian AC-like fold. Attempts to describe the structure of dimeric Rv1625c in its active dimeric form so far have failed: A structure of the full-length protein is not available, and the reported structures of the catalytic domain were either captured in an inactive monomeric form (25) or in a misfolded swapped dimer configuration (26).

Here, we report the structure of the cytosolic domain of the *Mycobacterium intracellulare* Cya homolog, revealing the organization of the helical domain of a membrane-integral adenylyl cyclase in an active nucleotide-bound conformation. We provide biochemical and biophysical evidence for the critical role of this domain in functional dimerization of the catalytic domains of the enzyme. Finally, our results provide an explanation for how disease-linked mutations in human cyclases may affect the function of the proteins.

Results

Structure of the Cytosolic Domain of *Mycobacterium intracellulare* Cya. To gain a deeper understanding of the membrane ACs, we crystallized the cytosolic domain of *M. intracellulare* Cya (Cya_{SOL}, 73% overall sequence identity with Rv1265c; 80% in the soluble portion; Fig. 1*A*). The crystallized construct retained enzymatic activity and the ability to bind a nucleotide analog, MANT-GTP (Fig. 1*B* and *SI Appendix*, Figs. S1 and S2; also see Fig. 4 *A* and *B*). We processed the data collected using cryo-preserved flash frozen crystals of Cya_{SOL} and solved the structure at a resolution of 2.7 Å (*SI Appendix*, Table S1). The asymmetric unit of Cya_{SOL} within the crystals is unusual, consisting of 11 monomers of Cya_{SOL} packed into a continuous fiber along the long axis of the crystalline lattice (Fig. 1*C*). Ten of the monomers form dimers within one asymmetric unit, with the 11th forming a dimer with a Cya_{SOL} monomer in an adjacent asymmetric unit (Fig. 1*C* and *SI Appendix*, Fig. S1). A portion of the electron density is poorly defined due to limited crystal contacts and whole domain motions of the protein (*SI Appendix*, Fig. S2*A*). The partially destabilized crystalline lattice is an intrinsic property of this crystal form, evident from the observed electron density features of an X-ray structure of Cya_{SOL} solved at 3.4-Å resolution using data collected at room temperature (*SI Appendix*, Fig. S2*B*). Using the anomalous scattering from Mn^{2+} ions in the active sites and the S atoms of Cys and Met residues in the well-ordered part of the map (*SI Appendix*, Figs. S1 *B* and *C* and S2 *A* and *C*), we were able to interpret the maps obtained from cryo-preserved and room temperature datasets and build a model of the complete cytosolic domain of Cya; all analysis below is focused on higher resolution data at 2.7-Å resolution.

The structure revealed a complex of Cya_{SOL} with MANT-GTP and Mn^{2+}, with two copies of substrate analog sandwiched between two catalytic domains in a closed active conformation (Fig. 1*D*). Interestingly, the two MANT-GTP molecules in the catalytic sites of each dimer are bound asymmetrically, with their bases oppositely oriented in the plane of domain interface (*SI Appendix*, Fig. S3).

A striking feature of the Cya_{SOL} structure is the helical domain: It is formed by two short helices that engage into a tight association in the juxtamembrane region of the catalytic domain (Fig. 1*E*). The residues spanning M212 to M226 form a two-stranded parallel coiled coil. The C-terminal portions of the two helical domains on the adjacent Cya monomers are highly conserved, and similar elements are observed in all nucleotidyl cyclases (*SI Appendix*, Fig. S4). The extreme N-terminal portions of the helical domain in the structure are disconnected from each other and are only partially resolved; this part of the protein is not making sufficiently strong contacts within the crystal, resulting in poor electron density features. Nevertheless, the quality of the electron density map corresponding to chains A–F together with the anomalous scattering data allowed us to build a high-quality model of the cytosolic domain of Cya.

Comparison with the AC–G Protein Complex, AC10, PAC, and the NO-Sensitive Cyclase Helical Domain. The structure of $AC5_{c1}$–$AC2_{c2}$–Gαs complex solved by Tesmer et al. (5) features no helical domain (*SI Appendix*, Fig. S4*B*; the domain was absent in the crystallized construct). Comparison of Cya_{SOL} with this complex does raise questions regarding the potential role of the helical domain in mammalian cyclase interaction with G protein subunits. Although this stretch of residues is short in Cya (LKSSS), the length of the region that links the helical and catalytic domains in the mammalian enzymes varies (*SI Appendix*, Fig. S4*A*). Thus, the proximity of the G protein binding interface to this region (indicated in *SI Appendix*, Fig. S4*B*) may have a functional significance for the mammalian membrane ACs.

Several other structures of type III cyclases are available to date, and comparisons of our Cya_{SOL} structure to some of them revealed remarkable conservation of the helical domain-like structural feature (*SI Appendix*, Fig. S4 *C–E*). The recently solved human AC10 (6) contains an N-terminal extension and a linker region between the catalytic domains that upon close inspection match perfectly the core helical domain found in our structure (*SI Appendix*, Fig. S4*C*).

Photoactivated AC from *Oscillatoria acuminata*, OaPAC, contains an N-terminal blue-light using FAD (BLUF) motif, part of which, assigned by the authors as helix α3-α4, resembles closely the helical domain of Cya (27) (*SI Appendix*, Fig. S4*D*). There are subtle differences between Cya and OaPAC, i.e., in the angle between the two helices forming the helix-turn-helix structure, which may have functional significance. For example, in the case of BLUF domain containing PAC, only a nucleotide-free structure is available. This raises the question of whether the difference in the helical domain regions in the nucleotide-free PAC and nucleotide-bound Cya is mechanistically significant. Addressing this issue using Cya_{SOL} is currently not possible, as it does not readily form dimers in the absence of nucleotides or the transmembrane domains.

Comparison of our structure to that of the isolated helical domain of soluble GC β1 subunit (28) reveals the similarity of the two domains. The availability of our structure makes it possible to refine the position of the helical domain of soluble GC with respect to its catalytic domain (example shown in *SI Appendix*, Fig.

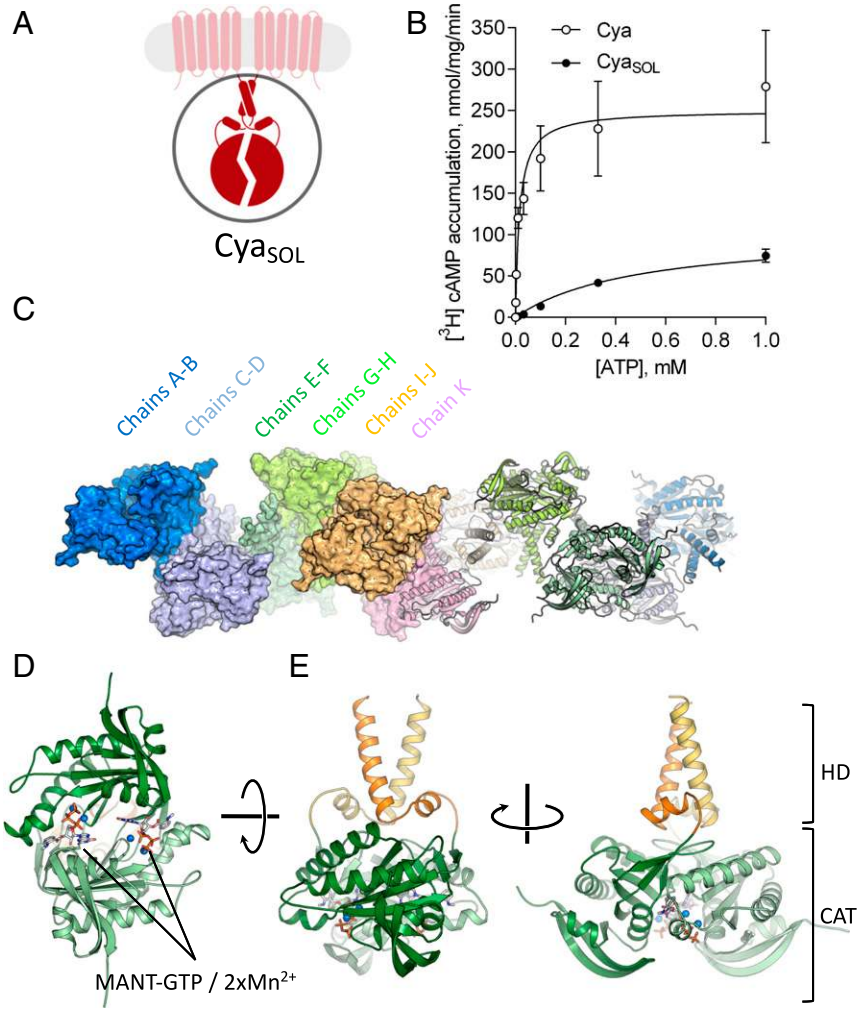

Fig. 1. Structure of the cytosolic domain of *M. intracellulare* Cya. (*A*) A schematic representation of Cya; cytosolic domain used for crystallization in this study is circled. (*B*) Enzymatic activity of purified full-length Cya and Cya$_{SOL}$; values are shown as mean ± SEM ($n = 4$), the K_m and V_{max} are shown in *SI Appendix*, Table S2. Different views of the structure of the soluble portion of Cya are shown. (*C*) Side view of two asymmetric units of Cya$_{SOL}$ crystals (space group C 1 2 1); 11 chains assemble into a continuous protein fiber along the long axis of the crystalline lattice; 10 of the monomers are assembled into 5 active dimers (chains A–J), with one (chain K) interacting with its counterpart in a neighbor asymmetric unit. (*D*) Structure of Cya$_{SOL}$ reveals two molecules of MANT-GTP ligand per dimer, with two Mn^{2+} ions bound per MANT-GTP. (*E*) The structure reveals the dimerized catalytic domain (CAT, colored forest and pale green) and the helical domain (HD; colored orange and light orange).

S4*E*). Considering the importance of the helical-catalytic domain interface region for soluble GC activation (11), the possibility of modeling the heterodimeric GC based on Cya may open new opportunities for structure-based exploration of coupling between the catalytic and auxiliary domains of nucleotidyl cyclases.

EPR Spectroscopy Confirms Cytosolic Domain Arrangement in the Full-Length Protein. To assess the behavior of the catalytic domain in the context of the full-length Cya, we purified the N328C mutant of Cya$_{\Delta Cys}$ (a Cys-free full-length Cya; *SI Appendix*, Fig. S5) and spin labeled this residue with MTSSL for EPR spectroscopy measurements (*SI Appendix*, Fig. S6*A*). The position of labeling was chosen such that any distances and changes measured could report on the motions of the whole domain (Fig. 2*A*). Labeling of this site in Cya$_{\Delta Cys}$ purified in detergent followed by continuous wave (CW) EPR spectroscopy confirmed that the spin label behaves as a rather rigidly attached probe (Fig. 2*B* and *SI Appendix*, Fig. S7*A*, *Bottom*), validating our strategy for using it as a reporter for whole domain movements. Consistent with the interlabel distance distribution simulated using the rotamer library approach (29) with our crystal structure as a template, the double electron-electron resonance (DEER) measurement in the presence of MANT-GTP ligand revealed presence of one strong interlabel distance peak at 61 ± 4 Å (Fig. 2 *C* and *D* and *SI Appendix*, Fig. S7 *A–G*). Moreover, essentially the same distance distribution was found for Cya in the absence of MANT-GTP. In contrast to the DEER experiments conducted in the context of the full-length Cya, analogous measurements on the isolated soluble domain showed a strong nucleotide dependence of its dimerization rate as judged by the DEER modulation depth (Fig. 2 *E* and *F* and *SI Appendix*, Fig. S7 *H–N*). The comparison of DEER traces in the presence and absence of MANT-GTP is consistent with substrate analog-dependent formation of Cya$_{SOL}$ dimers (Fig. 2 *E* and *F* and *SI Appendix*, Fig. S7 *H–N*). This observation confirms the specificity of the observed distance distribution and suggests that the full-length dimeric Cya complex is constitutively assembled and does not undergo large conformational rearrangements upon nucleotide binding.

Enzymatic Activity of Disease-Related Mutation Mimics in Cya. Several genetic diseases have recently been linked with mutations in nucleotidyl cyclases. In several cases, the mutations map directly

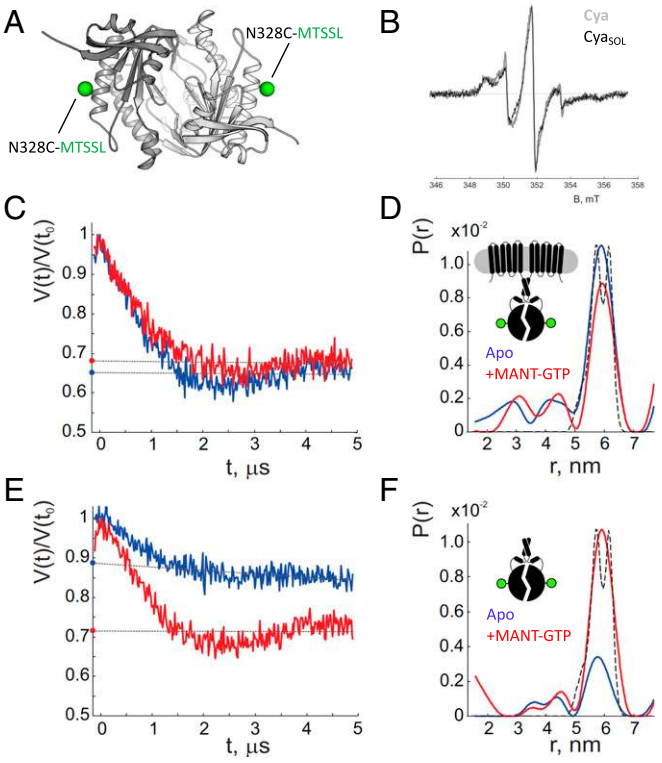

Fig. 2. EPR spectroscopy confirms the cytosolic domain arrangement in the full-length Cya. (*A*) A rigid position within the catalytic domain, N328, was chosen for mutation to Cys and spin labeling. (*B*) CW experiments show that the N328C position was successfully labeled and the position in the context of $Cya_{\Delta CYS}$ (gray) and $Cya_{SOL\Delta Cys}$ (black) is rather immobile. (*C*) Intensity-normalized Q-band DEER primary data of $Cya_{\Delta CYS}$-N328C. Details on acquisition and analysis of DEER data are in *SI Appendix*. (*D*) Simulated (dashed line) and experimentally determined distance distributions. The blue curves correspond to the apo state, while the red ones to the MANT-GTP bound; the Cya_{SOL} structure was used as a template for atom positions during simulations. (*E* and *F*) Same as in *C* and *D*, with data for the $Cya_{SOL\Delta Cys}$-N328C mutant; all observations in *C*–*F* are representative of three experiments. Dashed lines in *C* and *E* correspond to the decay functions used for background correction. From the crossings of the background decay functions with the normalized intensity axes (*y* axes) DEER modulation depths are determined (see *SI Appendix* for details).

to the helical domain-encoding sequences. For retGC1 (implicated in CORD6 and LCA-1), these amino acid substitutions include the following: E837D, R838P/H/G/C, E837D/R838C/T839M, T849A, and P858S (14, 16). In the case of AC5, the mutations R418W/Q and M1029K have been linked with FDFM and a variety of movement disorders (12). The availability of an X-ray structure of a cytosolic portion of a prototypical membrane-integral cyclase with its helical domain resolved led us to test whether similar mutations introduced in Cya could have functional consequences for the protein. The conservation of the helical domain among Cya and the cyclases implicated in disease is evident from sequence alignment (Fig. 3 *A* and *B*). If the helical domain configuration in Cya matches those in retGC1 and in AC5, Cya may prove to be a valuable model protein, helping us understand the effects of the disease-linked mutations on a molecular level.

We compared the enzymatic activity of purified full-length wild-type Cya to that of five mutants generated to recapitulate the human disease-related mutations in the context of a bacterial cyclase (Fig. 3 *A* and *B* and *SI Appendix*, Table S2). With respect to the catalysis rate of the wild-type Cya (Fig. 3*C* and *SI Appendix*, Table S2), a slight decrease in cAMP production was seen in the case of triple mutant (RAE-DCM) similar to the one in retGC1 implicated in LCA-1, while an increase, albeit insignificant, was observed in the E209W mutant mimicking the FDFM-linked AC5 substitution. The mutations closer to the core of the helical domain led to minor reduction of the cAMP accumulation rate; a statistically significant decrease was observed only in the M212K mutant. The most dramatic effect was observed for the P228S mutation, which abolished the ability of Cya to produce cAMP (Fig. 3*C*).

Stability of the Mutants. Functional differences observed in the mutants of Cya prompted us to evaluate their effect on protein stability. Some indication of protein stability could be inferred from the size exclusion chromatography experiments (*SI Appendix*, Fig. S11). We used the 7-diethylamino-3-(4′-maleimidylphenyl)-4-methylcoumarin (CPM)-based thermostability assays to determine the effects of helical domain mutations on the stability of the purified Cya proteins (Fig. 3*D* and *SI Appendix*, Fig. S12). Under the tested conditions, wild-type Cya in DDM showed an apparent melting temperature (t_m) of 54 °C, and the presence of MANT-GTP shifted the t_m to 73 °C. All of the mutations, except E209W, slightly destabilized the protein, which can be explained by the substitution of the hydrophobic core positions in the coiled coil in the N-terminal portion of the helical domain. The most robust destabilizing effect was observed with the P228S mutation. Interestingly, the E209W mutation stabilized the purified Cya, in the absence or presence of the ligand.

Both findings, i.e., the deleterious effect of P228S and the potentiating and stabilizing effect of E209W mutation, parallel the reported effects of the corresponding mutations in human proteins. The retGC1 P858S mutation (equivalent to P228S in Cya) severely affects cGMP production, whereas the FDFM-linked mutation in AC5, R418W (equivalent to E209W in Cya) potentiates the G protein-stimulated enzymatic activity of the enzyme. The results we obtained with Cya as a model system are consistent with the effects of mutations in human proteins.

Effects of the P228S Mutation in the Context of the Cya Cytosolic Domain. Encouraged by the experiments assessing the function and stability of the full-length Cya proteins, we endeavored to perform an in-depth analysis of the P228S mutation in the absence of the transmembrane domains. The rationale for this strategy was twofold: (*i*) the results might help us understand the behavior of the crystallized cytosolic domain; and (*ii*) biophysical characterization of isolated domains would allow us to address issues that may not be tackled experimentally in the context of a full-length membrane protein (e.g., dimerization of the catalytic domains). Activity measurements confirmed that the crystallized soluble cytosolic domain, Cya_{SOL}, possesses the ability to generate cAMP, albeit with a lower rate than observed in the case of the full-length protein (Figs. 1*B* and 4*A* and *SI Appendix*, Table S2). Removal of the helical domain or introduction of the P228S mutation resulted in a dramatic loss of enzymatic activity (Fig. 4*A*). Binding of MANT-GTP is preserved in all three constructs shown in Fig. 4*B*. In line with the experiments performed on full-length Cya, circular dichroism (CD)-based stability measurements of the isolated soluble domains revealed destabilization of the protein upon removal of the helical domain or introduction of the P228S mutation (*SI Appendix*, Fig. S13*B*).

AUC Confirms the Role of the Helical Domain in Functional Cyclase Domain Dimerization. To assess the effects of the helical domain on the ability of Cya_{SOL} to dimerize, we used analytical ultracentrifugation. In line with our DEER measurements on $Cya_{SOL\Delta Cys}$-N238C (Fig. 2 *E* and *F*), in the presence of MANT-GTP, the wild-type Cya_{SOL} was able to form dimeric species (Fig. 4*C*, *Top*). The profiles obtained at two different concentrations (0.3 and 1 mg/mL) for the wild-type protein in the apo state clearly indicate a tendency to form a dimer in a concentration-dependent manner. However, this tendency vanished upon removal or site-specific mutation (P228S)

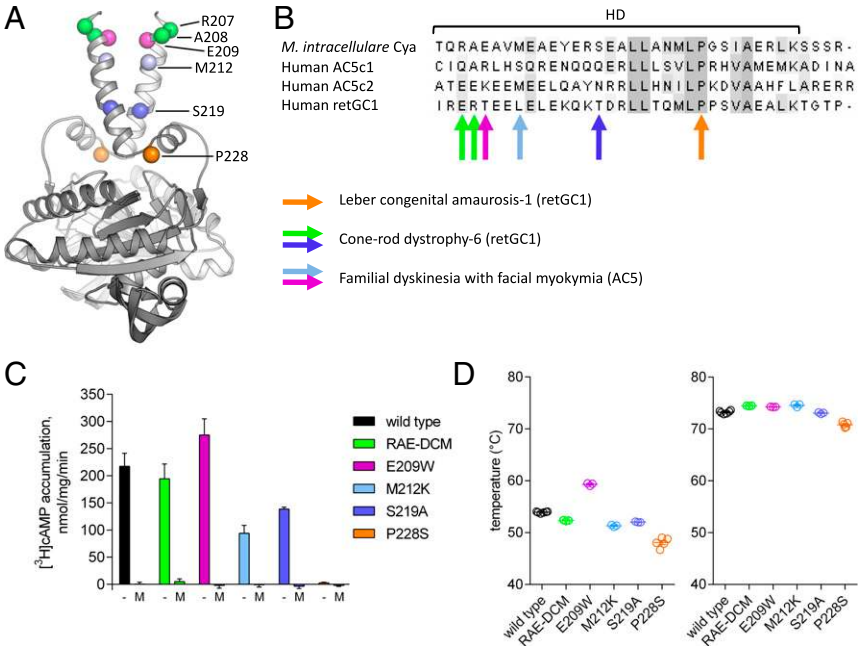

Fig. 3. Cya serves as a model for helical domain mutations implicated in genetic diseases in nucleotidyl cyclases. (*A* and *B*) Position of the mutants in the helical domain structure (*A*) and alignment of Cya with GCE and AC5 (c1 and c2) helical domains (*B*). Equivalently colored spheres and arrows indicate the positions of the affected mutations that are mapped on Cya_{SOL} structure in *A* or in sequence alignment in *B*. The alignment is shaded according to the BLOSUM62 score. (*C*) Enzymatic activity of full-length Cya, compared with five different mutants linked to human diseases grafted onto Cya construct. For each construct, the column on the *Left*, labeled with "−", indicates the assays performed in the absence of competitor; the column on the *Right*, labeled "M", indicates assays performed in the presence of MANT-GTP. Values are shown as mean ± SEM (n = 3–8); statistical significance was determined using one-way ANOVA followed by a Sidak's test (catalysis rates of M212K and P228S are significantly different from the wild type, with $P < 0.005$ and $P < 0.0001$, respectively). (*D*) CPM-based stability assay of the same purified mutant proteins, in the apo (*Left*) and in the MANT-GTP–bound (*Right*) state; values are shown as mean ± SEM (n = 3–6). Statistical significance was assessed using one-way ANOVA followed by a Sidak's test (all samples, apart from S219A in the MANT-GTP bound state, are significantly different from the wild-type; $P < 0.05$).

of the helical domain (Fig. 4*C*, *Middle* and *Bottom*). The ability of the P228S mutant to dimerize is intriguing in light of its inability to catalyze ATP to cAMP conversion, but this is consistent with the experiments that show preserved MANT-GTP binding in P228S Cya (or Cya_{SOL}) (Fig. 4*B*).

DEER Analysis Reveals Disruption of a Preassembled Full-Length Cya upon Introduction of the P228S Mutation. Analysis of the P228S mutation (in the context of the labeled $Cya_{\Delta Cys}$-N328C) using EPR spectroscopy showed a severe problem in domain assembly with or without bound ligand (*SI Appendix*, Figs. S6 and S8). This is evident from the broad distance distribution profiles, regardless of the presence of MANT-GTP in the sample. Although an apparently discrete long distance peak can be observed, its separation from the broad distribution at shorter distances is not significant and it does not perfectly match that seen in the spin-labeled $Cya_{\Delta Cys}$. The recorded DEER traces are consistent with two mutually connected properties of the sample: a deficiency in correct functional assembly of the labeled P228S mutant protein and a concomitant aggregation of the protein as a result of protein destabilization (Fig. 3*D* and *SI Appendix*, Fig. S6).

Discussion

The structure of the Cya cytosolic domain shows that the helical domain is an integral feature of nucleotidyl cyclases that has been conserved through evolution. The cyclase catalytic activity as such does not strictly require the presence of the helical domain, evident from previous studies on isolated domains of mammalian cyclases. Contingent on the formation of a native-like dimeric enzyme, stabilized by an activator, such as the activated G protein α subunit or forskolin, the cyclase activity can be reconstituted from isolated catalytic C1 and C2 domains of mammalian ACs, even in the absence of their helical domains (30). Nevertheless, adenylyl and guanylyl cyclases from prokaryotic and eukaryotic organisms contain this structural element, and it is clear from our data and from data on nucleotidyl cyclases published elsewhere that this domain is important for the mechanism of action of these enzymes. For example, hydrogen/deuterium exchange mass spectrometry analysis of NO-sensitive GC has shown that this region undergoes structural rearrangements associated with protein activation (11). The structure of the isolated helical domain from β1 subunit of soluble GC featured two pairs of antiparallel helices stacked against each other (28), making a case for both parallel and antiparallel helical domain arrangements. The parallel helical domain structure has been argued to be the only possible configuration based on the low-resolution, single-particle reconstruction of soluble GC (10). Despite the existence of conflicting evidence for the role of the helical domain in receptor GCs, such as retGC1 (8, 31, 32), it has generally been accepted that the domain must be involved in protein dimerization. Furthermore, the retGC1 helical domain contributes to the interface between the cyclase and the activator proteins, GCAP1 and GCAP2 (8). A motif very closely resembling the helical domain described here is present in the AC10 structure (6), although its functional significance has until now been unclear. The biochemical role of this domain in integral membrane G protein-sensitive ACs has been largely unexplored.

Identification of genetic disease-linked single-nucleotide polymorphisms mapping to the helical domains of retGC1 and AC5 has put the spotlight on these regions of the enzymes. Functionally, the mutations in the two human proteins have opposing consequences: In AC5, the mutations in this region potentiate the ability of the enzyme to elicit G protein-induced response (12, 13), whereas the mutations in retGC1 abolish cGMP generation by this protein (14, 16, 33). The effects of at least some of these mutations

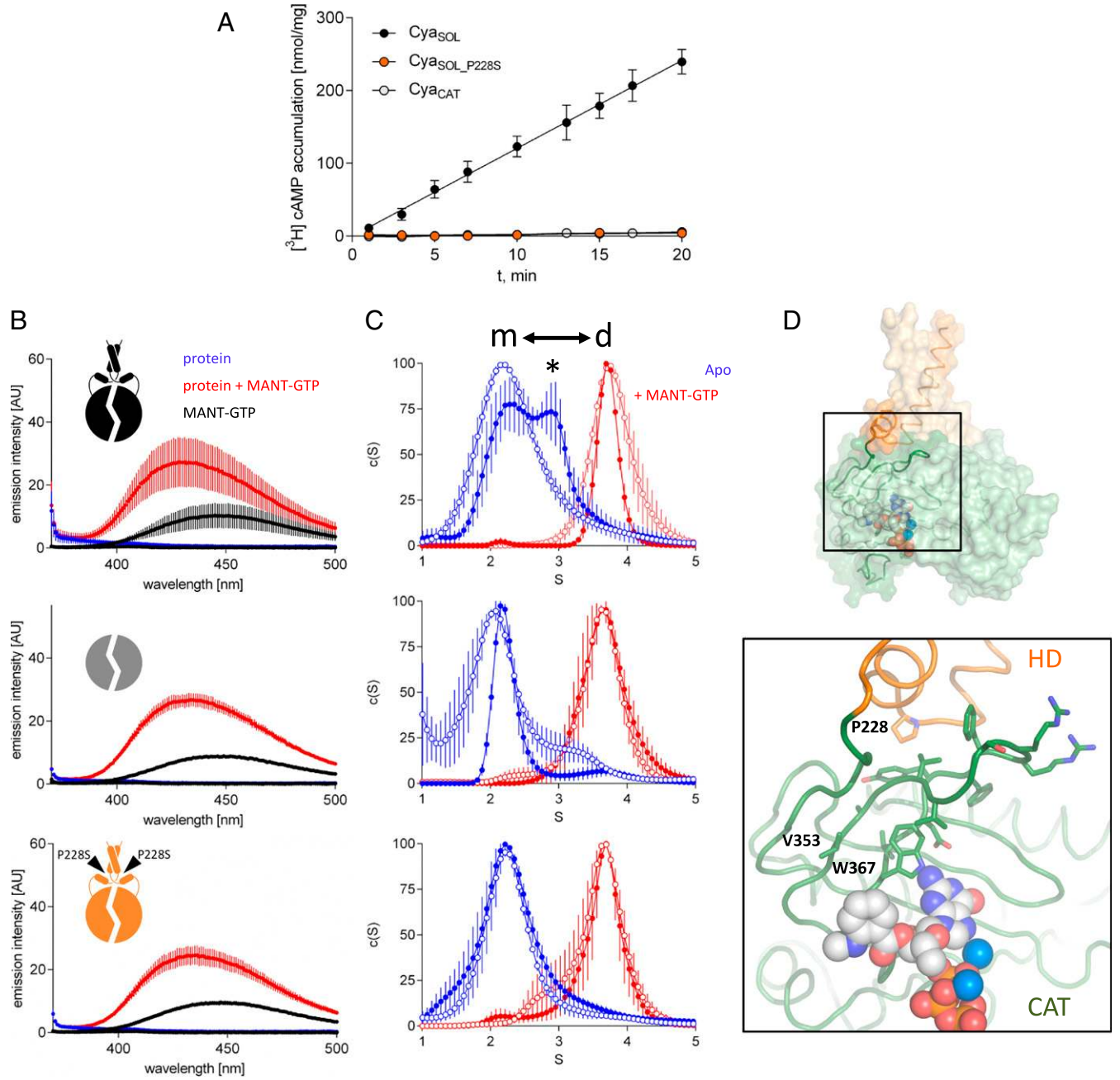

Fig. 4. The P228S mutation disrupts the enzymatic activity but preserves the nucleotide interactions with the catalytic domains. (*A*) Ability of the Cya_{SOL} to produce cAMP is severely impaired by removal of the helical domain or by introduction of a P228S mutation. (*B*) Fluorescence-based MANT-GTP binding assay confirms that all three constructs are capable of binding the nucleotide analog. Excitation wavelength was 350 nm; emission was recorded in the range of 370–500 nm. *Inset* sketches describe each construct, colored according to the colors in *A*. (*C*) Normalized analytical ultracentrifugation (AUC) profiles of the three constructs; AUC was performed at two protein concentrations, 0.3 mg/mL (open circles) and 1 mg/mL (filled circles), in the absence (blue) or presence of MANT-GTP (red). Cya_{SOL} was compared with the P228S mutant and the catalytic domain only. (*Top*) A propensity to dimerize in the absence of nucleotide is evident from a discrete peak in the Cya_{SOL} sample (asterisk) and only at 1 mg/mL; the appearance of this intermediate peak at a higher protein concentration is indicative of a monomer-dimer equilibrium. (*Middle* and *Bottom*) Disruption of the helical domain by truncation or P228S mutation abolishes dimerization. Monomers and dimers are indicated by "m" and "d," linked by an arrow. For all experiments, values are shown as mean ± SEM ($n = 3$). (*D*) Interface between the Cya helical domain and its catalytic site. The surface representation depicts the shape of Cya_{SOL} dimer. A chain of the Cya_{SOL} monomer is shown in ribbon representation; MANT-GTP and $2xMn^{2+}$ ions are represented as spheres; Mn^{2+} ions are represented as blue spheres. The boxed area indicates side chains of P228 in the helical domain (HD) and the loop formed by residues V353-W367, which acts as the interface between the helical domain and the catalytic domain (CAT).

can now be rationalized based on the structural evidence and on the biophysical analysis of the Cya mutants described here. The relatively mild functional consequences of the mutations in the N-terminal portion of the helical domain (Fig. 3) suggest that these residues are at the protein surface in the full-length Cya. Substitution of these residues in the full-length Cya has little effect on the ability of the protein to generate cAMP. Mutations closer to the core of the helical domain modulate the enzymatic activity of the protein, consistent with the proposed role of the helical domain in protein dimerization. Finally, perturbation of the helical

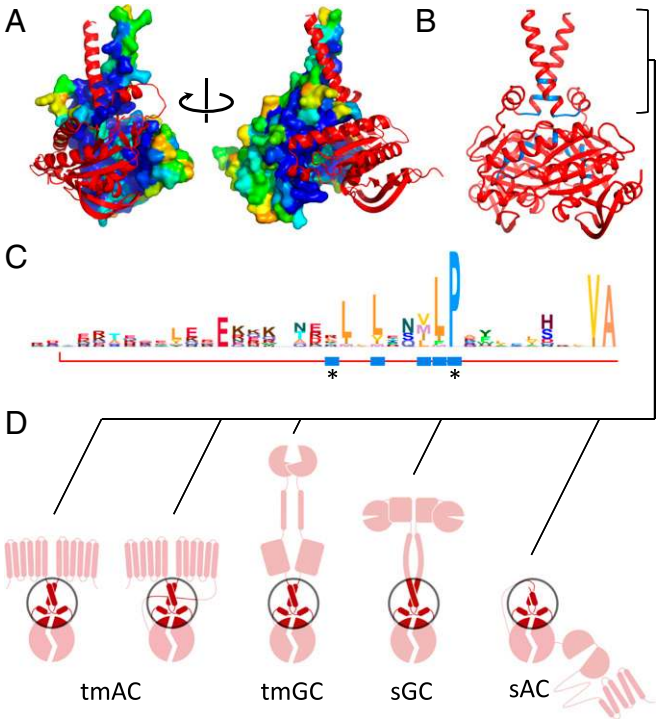

Fig. 5. Conservation of helical domain core in nucleotidyl cyclases across species and protein families. (*A*) Cya_{SOL} dimer shown with one monomer in surface representation and the other shown in ribbon representation. Interface analysis using Eppic (46) reveals strong conservation of interface residues within close homologs of Cya. Sequence identity cutoff was kept at 30%, but similar results were obtained using 15–50% identity cutoff. The color code reflects the sequence entropy, as defined in Eppic: blue, low entropy/high conservation; red, high entropy/low conservation (Eppic database statistics for this search: UniProt_2016_07 and PDB release of 18–10-2016). (*B*) Map of the core residues (colored in blue) at the Cya_{SOL} dimer interface, as defined in Eppic (>95% buried surface). The helical domain contributes substantially to the dimer interface residues of Cya_{SOL}, with 9 of 23 core residues mapped to the helical domain interface. (*C*) A high conservation of the helical domain core features is revealed by HMMER search (www.hmmer.org) (47) in mammalian proteome database using *M. intracellulare* Cya cytosolic domain sequence as a search template. The HMM logo was generated from the HMMER multiple sequence alignment output using Skylign (www.skylign.org). The red line underlining the HMM logo indicates the corresponding residues resolved in Cya_{SOL} structure; blue rectangles indicate core residues (as shown in *B*). Asterisks indicate residues implicated in genetic diseases upon mutation in retGC1 (detailed in the text). (*D*) The helical domain is conserved across protein families and architectures and is present in bacterial and mammalian membrane ACs ("tmAC"; adjacent sketches represent mycobacterial Rv1625c/Cya and mammalian AC1–9), receptor GCs ("tmGC"), NO-sensitive soluble GC ("sGC"), and soluble AC10 ("sAC").

domain hinge region (P228S) destabilizes the full-length Cya and clearly interferes with catalytic domain assembly, as judged by cAMP accumulation experiments, thermostability measurements, analytical centrifugation, and EPR spectroscopy. Remarkably, the ability to bind the nucleotide is not lost in the P228S mutant (Fig. 4*B* and *SI Appendix*, Fig. S10); the mutated protein is capable of binding an ATP analog, and the catalytic domains undergo substrate-induced dimerization. It is thus possible that Cya, as well as other nucleotidyl cyclases, feature a functionally important interface between the catalytic sites and the helical domain. A single peptide loop, corresponding to a stretch of residues 353–367 of a Cya monomer, separates the helical domain from the catalytic site (Fig. 4*D*). It is possible that the P228S mutation does not only destabilize the helical domain, but also exerts additional constraints on the underlying catalytic site via this interface.

Asymmetric binding of the substrate nucleotide to the AC catalytic site has been observed previously in the nucleotide-bound state of *M. tuberculosis* Rv1900c, with only one ATP analog molecule bound to the cyclase catalytic dimer (34). A recent study of nucleotide binding site specificity in another AC, *M. avium* Ma1120, revealed that this protein tolerates a wide range of bound nucleotide conformations in the binding pocket (35). Consistent with these earlier studies, our results are suggestive of how the binding site may have evolved from bacteria to mammals: whereas bacterial homodimeric cyclases can process two nucleotide molecules, in mammals one of the binding sites within the heterodimeric catalytic domain accommodates an allosteric ligand such as the AC activator forskolin. The innate flexibility of the substrate binding site in Cya-like ancestral precursors of the mammalian ACs may have facilitated the emergence of the allosteric site in the course of evolution.

The results of our EPR experiments support an important conclusion about the constitutive functional assembly of the Cya dimer: Although our crystal structure in the presence of nucleotide represents the substrate bound-state of full-length Cya, the conformation of its apo state may not be very different. This is consistent with small structural changes seen in AC10 structures, where minimal movements of the protein are observed under a variety of conditions (6, 36), with and without substrates, ions, and allosteric modulators. Thus, if structural elements N-terminal with respect to the catalytic domain were to exert effects on the catalytic function of the protein, the physical action required would be very subtle. It is noteworthy that sequencing of the first mammalian membrane AC prompted suggestions that these proteins resemble membrane channels or transporters (37). For example, the architecture of the membrane cyclases is indeed reminiscent of the mammalian ABC exporters, which also feature 12 TM domains and 2 ATP-binding soluble domains (38). Bacterial homologs of the ABC exporters are half-transporters, with only six TM domains and a single nucleotide-binding domain; this parallels the case of Cya (or Rv1625c) and mammalian ACs. Structural and biochemical studies in recent years revealed the structures of ABC transporters and showed a range of conformations that these proteins adopt during the cycles of nucleotide binding/hydrolysis/dissociation, coupled to substrate translocation (38). If the early predictions of structural similarities between ACs and transporters were correct, one could expect similarly large conformational rearrangements involving whole domain motions in the membrane cyclases in response to nucleotide binding. Our results indicate that this is likely not the case, pointing toward a constitutively dimerized enzyme that is brought together by the TM domains. The helical domain, at the boundary between the TM and the catalytic domains of the protein, contributes to the dimerization interface and appears to have a key role in the assembly of a functionally active dimeric state of the protein. It is possible that regulation of cyclase activity in the human nucleotidyl cyclases is exerted via their helical or catalytic domains with minute local conformational changes, as is suggested by our EPR results using Cya as a model cyclase.

In conclusion, our results indicate that the helical domain is a highly conserved integral element of nucleotidyl cyclases that plays an important role in the mechanism of these domains across protein classes and functions. This domain may have coevolved with the type III cyclase fold as an essential structural motif, carrying with it important assembly- and regulation-related functions and adapting to the individual architectural context of each nucleotidyl cyclase (Fig. 5). This assertion is in line with the recent biochemical and bioinformatics analysis that described the helical domain as a signal transducer element important for functionally coupling the membrane-bound and the catalytic portions of type III adenylyl and guanylyl cyclases (39). Future work on structures and mechanisms of full-length membrane-integral and soluble

nucleotidyl cyclases will help define the role of each regulatory domain of these multifaceted enzymes.

Materials and Methods

Protein purification and crystallization was performed using standard vapor diffusion methodology. Protein was purified by NiNTA affinity chromatography following the vendor recommendations, and the 10xHis tag was removed by cleavage with 3C protease. The final purification step, size exclusion chromatography in a buffer composed of 20 mM Tris and 50 mM NaCl, 0.5 mM EDTA was performed before protein concentration and crystallization. Crystals were grown and optimized using the in-house crystallization facility; the best crystals were obtained using a mixture of PEG 1000 and PEG 8000, 200 mM Li_2SO_4, and 100 mM Na-cacodylate buffer (pH 6.5) in the mother liquor, with protein supplemented with 5 mM $MnCl_2$ and 1 mM MANT-GTP. The crystals diffracted to 2.7-Å resolution at the PXI/III beamlines at Swiss Light Source (SLS). Crystallographic data processing was performed using XDS (40), and the structure was solved using MR-SAD in Phenix (41). The data were scaled to 2.7 Å and refined using Phenix and Buster, Global Phasing (42). The room temperature dataset was scaled to 3.4 Å, and structure was refined using Phenix. Fluorescence-based ligand binding assays were performed as described previously (43). Enzymatic activity was measured using a single column method (44) with minor modifications. Protein stability of purified full-length Cya constructs was measured using the CPM assay; in the case of soluble domains, stability was determined using CD spectroscopy. Dimerization of Cya_{CAT}, Cya_{SOL}, and Cya_{SOL}-P228S mutant was assessed using AUC following the standard procedures, as detailed in *SI Appendix*. Site-directed spin labeling of $Cya_{\Delta Cys}$-N328C, $Cya_{\Delta Cys}$-N328C-P228S, and $Cya_{SOL\Delta Cys}$-N328C with MTSL reagent and EPR spectroscopy followed the procedures established for other membrane proteins (45) with some modifications. Simulated distance distribution between spin labels were obtained with the rotamer library approach (29). A detailed description of all experimental procedures is provided in *SI Appendix, SI Methods and Materials*.

ACKNOWLEDGMENTS. We thank May Sharpe and Laura Vera (SLS crystallization facility) for assistance in protein crystallization; the staff at PXI and PXIII beamlines at SLS for support during X-ray data collection and processing; Ziva Vuckovic and Franziska Heydenreich (Paul Scherrer Institute, PSI) for assistance in performing the biophysical experiments; Guido Capitani (PSI) for fruitful discussions on processing of the crystallographic data; and Adriana Weinert, Dmitry Veprintsev (PSI), and Christopher G. Tate (Medical Research Council Laboratory of Molecular Biology) for providing critical comments. This work was supported by Swiss National Science Foundation (SNF) Professorship Grant 150665.

1. Sinha SC, Sprang SR (2006) Structures, mechanism, regulation and evolution of class III nucleotidyl cyclases. *Rev Physiol Biochem Pharmacol* 157:105–140.
2. Kamenetsky M, et al. (2006) Molecular details of cAMP generation in mammalian cells: A tale of two systems. *J Mol Biol* 362:623–639.
3. Steegborn C (2014) Structure, mechanism, and regulation of soluble adenylyl cyclases–Similarities and differences to transmembrane adenylyl cyclases. *Biochim Biophys Acta* 1842:2535–2547.
4. Pierre S, Eschenhagen T, Geisslinger G, Scholich K (2009) Capturing adenylyl cyclases as potential drug targets. *Nat Rev Drug Discov* 8:321–335.
5. Tesmer JJ, Sunahara RK, Gilman AG, Sprang SR (1997) Crystal structure of the catalytic domains of adenylyl cyclase in a complex with Gsalpha.GTPgammaS. *Science* 278:1907–1916.
6. Kleinboelting S, et al. (2014) Crystal structures of human soluble adenylyl cyclase reveal mechanisms of catalysis and of its activation through bicarbonate. *Proc Natl Acad Sci USA* 111:3727–3732.
7. Potter LR (2005) Domain analysis of human transmembrane guanylyl cyclase receptors: Implications for regulation. *Front Biosci* 10:1205–1220.
8. Peshenko IV, Olshevskaya EV, Dizhoor AM (2015) Dimerization domain of retinal membrane guanylyl cyclase 1 (RetGC1) is an essential part of guanylyl cyclase-activating protein (GCAP) binding interface. *J Biol Chem* 290:19584–19596.
9. Derbyshire ER, Marletta MA (2012) Structure and regulation of soluble guanylate cyclase. *Annu Rev Biochem* 81:533–559.
10. Campbell MG, Underbakke ES, Potter CS, Carragher B, Marletta MA (2014) Single-particle EM reveals the higher-order domain architecture of soluble guanylate cyclase. *Proc Natl Acad Sci USA* 111:2960–2965.
11. Underbakke ES, et al. (2014) Nitric oxide-induced conformational changes in soluble guanylate cyclase. *Structure* 22:602–611.
12. Chen YZ, et al. (2012) Autosomal dominant familial dyskinesia and facial myokymia: Single exome sequencing identifies a mutation in adenylyl cyclase 5. *Arch Neurol* 69: 630–635.
13. Chang FC, et al. (2016) Phenotypic insights into ADCY5-associated disease. *Mov Disord* 31:1033–1040.
14. Zhao X, et al. (2013) A novel GUCY2D mutation in a Chinese family with dominant cone dystrophy. *Mol Vis* 19:1039–1046.
15. Kitiratschky VB, et al. (2008) Mutation analysis identifies GUCY2D as the major gene responsible for autosomal dominant progressive cone degeneration. *Invest Ophthalmol Vis Sci* 49:5015–5023.
16. Tucker CL, et al. (2004) Functional analyses of mutant recessive GUCY2D alleles identified in Leber congenital amaurosis patients: Protein domain comparisons and dominant negative effects. *Mol Vis* 10:297–303.
17. Li L, et al. (2011) Detection of variants in 15 genes in 87 unrelated Chinese patients with Leber congenital amaurosis. *PLoS One* 6:e19458.
18. Chen YZ, et al. (2014) Gain-of-function ADCY5 mutations in familial dyskinesia with facial myokymia. *Ann Neurol* 75:542–549.
19. Tesmer JJ, et al. (2000) Molecular basis for P-site inhibition of adenylyl cyclase. *Biochemistry* 39:14464–14471.
20. Tesmer JJ, et al. (1999) Two-metal-ion catalysis in adenylyl cyclase. *Science* 285: 756–760.
21. Bieger B, Essen LO (2001) Structural analysis of adenylate cyclases from Trypanosoma brucei in their monomeric state. *EMBO J* 20:433–445.
22. Topal H, et al. (2012) Crystal structure and regulation mechanisms of the CyaB adenylyl cyclase from the human pathogen Pseudomonas aeruginosa. *J Mol Biol* 416: 271–286.
23. Guo YL, Seebacher T, Kurz U, Linder JU, Schultz JE (2001) Adenylyl cyclase Rv1625c of Mycobacterium tuberculosis: A progenitor of mammalian adenylyl cyclases. *EMBO J* 20:3667–3675.
24. Beltz S, Bassler J, Schultz JE (2016) Regulation by the quorum sensor from Vibrio indicates a receptor function for the membrane anchors of adenylate cyclases. *Elife* 5: e13098.
25. Ketkar AD, Shenoy AR, Ramagopal UA, Visweswariah SS, Suguna K (2006) A structural basis for the role of nucleotide specifying residues in regulating the oligomerization of the Rv1625c adenylyl cyclase from M. tuberculosis. *J Mol Biol* 356:904–916.
26. Barathy D, Mattoo R, Visweswariah S, Suguna K (2014) New structural forms of a mycobacterial adenylyl cyclase Rv1625c. *IUCrJ* 1:338–348.
27. Ohki M, et al. (2016) Structural insight into photoactivation of an adenylate cyclase from a photosynthetic cyanobacterium. *Proc Natl Acad Sci USA* 113:6659–6664.
28. Ma X, Beuve A, van den Akker F (2010) Crystal structure of the signaling helix coiled-coil domain of the beta1 subunit of the soluble guanylyl cyclase. *BMC Struct Biol* 10:2.
29. Polyhach Y, Bordignon E, Jeschke G (2011) Rotamer libraries of spin labelled cysteines for protein studies. *Phys Chem Chem Phys* 13:2356–2366.
30. Whisnant RE, Gilman AG, Dessauer CW (1996) Interaction of the two cytosolic domains of mammalian adenylyl cyclase. *Proc Natl Acad Sci USA* 93:6621–6625.
31. Ramamurthy V, et al. (2001) Interactions within the coiled-coil domain of RetGC-1 guanylyl cyclase are optimized for regulation rather than for high affinity. *J Biol Chem* 276:26218–26229.
32. Duda T, Pertzev A, Sharma RK (2012) Differential Ca(2+) sensor guanylate cyclase activating protein modes of photoreceptor rod outer segment membrane guanylate cyclase signaling. *Biochemistry* 51:4650–4657.
33. Dharmaraj SR, et al. (2000) Mutational analysis and clinical correlation in Leber congenital amaurosis. *Ophthalmic Genet* 21:135–150.
34. Sinha SC, Wetterer M, Sprang SR, Schultz JE, Linder JU (2005) Origin of asymmetry in adenylyl cyclases: Structures of Mycobacterium tuberculosis Rv1900c. *EMBO J* 24: 663–673.
35. Bharambe NG, et al. (2016) Substrate specificity determinants of class III nucleotidyl cyclases. *FEBS J* 283:3723–3738.
36. Kleinboelting S, van den Heuvel J, Steegborn C (2014) Structural analysis of human soluble adenylyl cyclase and crystal structures of its nucleotide complexes-implications for cyclase catalysis and evolution. *FEBS J* 281:4151–4164.
37. Krupinski J, et al. (1989) Adenylyl cyclase amino acid sequence: Possible channel- or transporter-like structure. *Science* 244:1558–1564.
38. Locher KP (2016) Mechanistic diversity in ATP-binding cassette (ABC) transporters. *Nat Struct Mol Biol* 23:487–493.
39. Ziegler M, et al. (2017) Characterization of a novel signal transducer element intrinsic to class IIIa/b adenylate cyclases and guanylate cyclases. *FEBS J* 284:1204–1217.
40. Kabsch W (2010) Xds. *Acta Crystallogr D Biol Crystallogr* 66:125–132.
41. Adams PD, et al. (2010) PHENIX: A comprehensive Python-based system for macromolecular structure solution. *Acta Crystallogr D Biol Crystallogr* 66:213–221.
42. Smart OS, et al. (2012) Exploiting structure similarity in refinement: Automated NCS and target-structure restraints in BUSTER. *Acta Crystallogr D Biol Crystallogr* 68: 368–380.
43. Hübner M, et al. (2011) Structural basis for the high-affinity inhibition of mammalian membranous adenylyl cyclase by 2′,3′-o-(N-methylanthraniloyl)-inosine 5′-triphosphate. *Mol Pharmacol* 80:87–96.
44. Alvarez R, Daniels DV (1990) A single column method for the assay of adenylate cyclase. *Anal Biochem* 187:98–103.
45. Joseph B, Korkhov VM, Yulikov M, Jeschke G, Bordignon E (2014) Conformational cycle of the vitamin B12 ABC importer in liposomes detected by double electron-electron resonance (DEER). *J Biol Chem* 289:3176–3185.
46. Duarte JM, Srebniak A, Schärer MA, Capitani G (2012) Protein interface classification by evolutionary analysis. *BMC Bioinformatics* 13:334.
47. Finn RD, Clements J, Eddy SR (2011) HMMER web server: Interactive sequence similarity searching. *Nucleic Acids Res* 39:W29–W37.